UNCLASSIFIED

AD _ 405 874 _

DEFENSE DOCUMENTATION CENTER

FOR

SCIENTIFIC AND TECHNICAL INFORMATION

CAMERON STATION, ALEXANDRIA, VIRGINIA

UNCLASSIFIED

ESD-TDR-63-181   PM-22 #17

RADAR SYSTEMS AND TECHNIQUES DEPARTMENT
MICROWAVE TECHNIQUES SUBDEPARTMENT QPR
JULY 1, 1962 — SEPTEMBER 30, 1962

TECHNICAL DOCUMENTARY REPORT NO. ESD-TDR-63-181

May 1963

Microwave Techniques Subdepartment

Prepared for

DIRECTORATE OF RADAR AND OPTICS

ELECTRONIC SYSTEMS DIVISION

AIR FORCE SYSTEMS COMMAND

UNITED STATES AIR FORCE

L. G. Hanscom Field, Bedford, Massachusetts

Prepared by

THE MITRE CORPORATION
Bedford, Massachusetts
Contract AF33(600)-39852 Projects 602 and 750

RADAR SYSTEMS AND TECHNIQUES DEPARTMENT
MICROWAVE TECHNIQUES SUBDEPARTMENT QPR
JULY 1, 1962 — SEPTEMBER 30, 1962

TECHNICAL DOCUMENTARY REPORT NO. ESD-TDR-63-181

May 1963
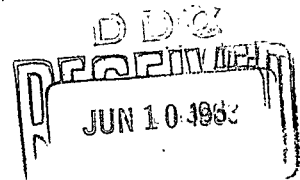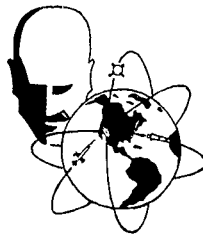
Microwave Techniques Subdepartment

Prepared for

DIRECTORATE OF RADAR AND OPTICS

ELECTRONIC SYSTEMS DIVISION

AIR FORCE SYSTEMS COMMAND

UNITED STATES AIR FORCE

L. G. Hanscom Field, Bedford, Massachusetts
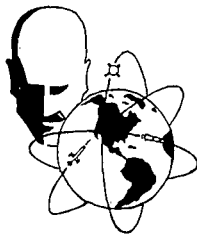
Prepared by

THE MITRE CORPORATION
Bedford, Massachusetts
Contract AF33(600)-39852 Projects 602 and 750

FOREWORD

This report represents the efforts of the following members of
the Microwave Techniques Subdepartment of The MITRE Cor-
poration's Radar Systems and Techniques Department.

J. H. Phillips, Subdepartment Head

W. M. Bridge   A. P. Murphy
D. E. Cozzens   R. L. Severance
C. J. Ferraro   R. J. Snay
R. D. Gallagher   P. M. Ware
A. L. Murphy

ABSTRACT

This document reports the progress of the Microwave Techniques
Subdepartment from July 1, 1962 to September 30, 1962. The
work of the Subdepartment centers on the design, fabrication and
evaluation of microwave techniques and components which have
application to long-range radar and communication problems.

CONTENTS

v

THE MICROWAVE TECHNIQUES SUBDEPARTMENT

INTRODUCTION

The work reported in this document is supported under Project 750, Radar and Communication Techniques. To date, the majority of the work conducted in the subdepartment has been performed under this project. Work on other projects is reported separately in the form of internal MITRE documents.

The subdepartment's activities are divided into two major categories: Antenna Studies and Solid-State Microwave Studies. In addition, the subdepartment furnishes microwave componentry for the D-22 experimental radar.

During this quarter, the radar was put on the air. The parametric amplifier developed by the subdepartment, performed satisfactorily with the system. The second-site parametric amplifier was installed at Boston Hill, and a brief course in operating procedures given to site personnel.

PARAMETRIC AMPLIFIER STUDIES

L-Band Parametric Amplifier

The components for the low-noise L-band parametric amplifier were completed, tested and assembled into a working amplifier. Preliminary investigations showed stable gains in excess of 30 db and bandwidths greater than 20 mc at 20-db gain. The noise figure was measured at approximately 4 to 5 db. However, this measurement was obtained while the varactor was rectifying the pump current, and it is believed the shot noise of this forward current may have caused the relatively poor noise figure. Modifications being incorporated should provide a high-gain bandwidth product without rectified pump current.

Two filters developed for this amplifier are of particular interest. The sliding coaxial filter, discussed in PM-22 #14, now provides a rejection of greater than 35 db over a band of frequencies from 9.6 to 12.0 kmc and a VSWR of less than 1.2 over a signal band of 1250 to 1400 mc.

2

An impedance transforming waveguide filter was developed to provide a matched transition from the full-height X-band waveguide to the 0.055-inch reduced-height waveguide necessary for the parametric amplifier. It was designed to provide a Butterworth insertion loss characteristic over a prescribed band of pump frequencies, and to provide a given rejection to a particular out-of-band-frequency. The design is very similar to that set forth in MTS-4,[1] except that the first quarter-wave inverter is synthesized as an abrupt step in waveguide height, which is approximately equivalent to an abrupt change in characteristic impedance. The remaining quarter-wave inverters are synthesized in the usual form as inductive posts. The results of using the three-section impedance transforming filter in the L-band parametric amplifier are shown in Fig. 1. The design center frequency is 11.50 kmc with a bandwidth of 614 mc, while the observed center frequency was 11.56 kmc and the observed bandwidth was 580 mc. The filter was designed to have greater than 20-db rejection for frequencies below 10.8 kmc, and a rejection of 44 db was measured at 10.4 kmc.

Fig. 1 Reflection Loss of Filter

Solid-State Source

    Both the X-band pump source and the pump limiter were delivered during the quarter. The complete specifications for the solid-state source, previously outlined, are detailed in Table I.

Table I

Specifications for All-Solid-State X-Band Pump Power Source*

Characteristics	Ranges of Values
Output Frequency	11.5 kmc
Output Power	150 mw min
Output Amplitude Stability	± 0.5 db over temperature range
Spurious Outputs	40 db min for any response within ± 100 mc of output frequency; 30 db for all other responses
Input Power Requirement	48 v at 600 ma; 0.1% regulation 28 v at 250 ma; 0.1% regulation
Frequency Stability	± 1 part in 10^5
Frequency Trim Range	± 0.001%
Load VSWR	1.25 max
Temperature Range	-30° to +55° C
Size	8 x 6 x 5 in. max, exclusive of mounting protuberances
Weight	8 lb max
Output Flange	UG-39/u

*Manufactured by Microwave Associates, Inc.
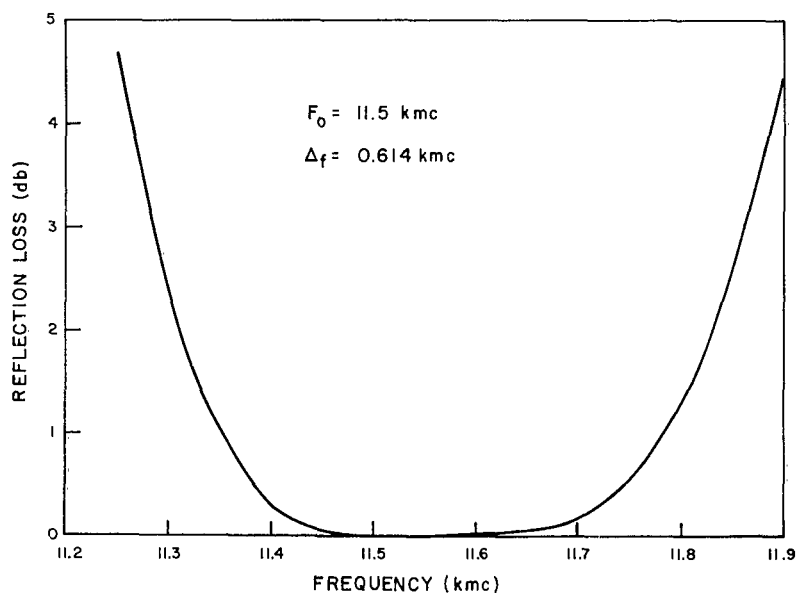
Solid-State Source

Both the X-band pump source and the pump limiter were delivered during the quarter. The complete specifications for the solid-state source, previously outlined, are detailed in Table I.

Table I

Specifications for All-Solid-State X-Band Pump Power Source*

Characteristics	Ranges of Values
Output Frequency	11.5 kmc
Output Power	150 mw min
Output Amplitude Stability	± 0.5 db over temperature range
Spurious Outputs	40 db min for any response within ± 100 mc of output frequency; 30 db for all other responses
Input Power Requirement	48 v at 600 ma; 0.1% regulation 28 v at 250 ma; 0.1% regulation
Frequency Stability	± 1 part in 10^5
Frequency Trim Range	$\pm 0.001\%$
Load VSWR	1.25 max
Temperature Range	-30° to $+55^\circ$ C
Size	8 x 6 x 5 in. max, exclusive of mounting protuberances
Weight	8 lb max
Output Flange	UG-39/u

*Manufactured by Microwave Associates, Inc.

4

The block diagram of the X-band source is shown in Fig. 2. An oven-controlled crystal oscillator generates a stable 30-mc signal. This signal is amplified, doubled, and again amplified by transistor stages to a 12-watt level. Three varactor quadruplers in cascade multiply the frequency to 3840 mc. The 3840-mc signal is filtered and multiplied to 11520 mc in a varactor trippler. The X-band signal then is further filtered to suppress any undesired harmonics.
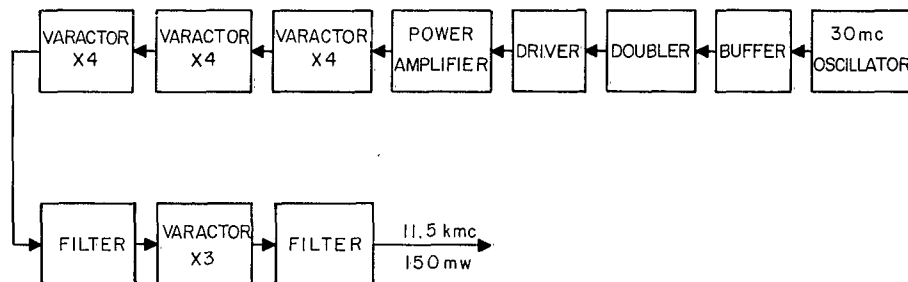

Fig. 2   Block Diagram of X-Band Source

Diode Characteristics at Microwave Frequencies

The diodes used in this measurement are RCA point-contact varactors and microstate graded-junction varactors. Both are gallium arsenide diodes with reported cutoff frequencies above 200 kmc.

First, attempts were made to measure the diode characteristics at 1300 mc. A 50-ohm coaxial jig (Fig. 3) was constructed to hold the diode and to provide means of applying d-c bias.[2]   The circuit used to measure the diode Q is shown in Figure 4. With the tuner adjusted for match at any bias voltage (in this case, 0 volts), the bias was varied in both positive and negative directions. The impedances are shown in Figs. 5 and 6.

The operating frequency of the jig was insufficient for the measurement desired. If equations for the diode Q and for the cutoff frequency f_c are established, this can be demonstrated mathematically.

DIODE

BYPASS
CAPACITOR

Fig. 3 Cross Section of 50-ohm
Coaxial Jig Used in Measure-
ment of Diode Characteristics
at 1300 mc

BIAS
TERMINAL

SIGNAL
SOURCE

| DETECTOR | ISOLATOR | SLOTTED LINE | TUNER | DIODE IN TEST JIG | D-C BIAS |

VSWR
AMPLIFIER
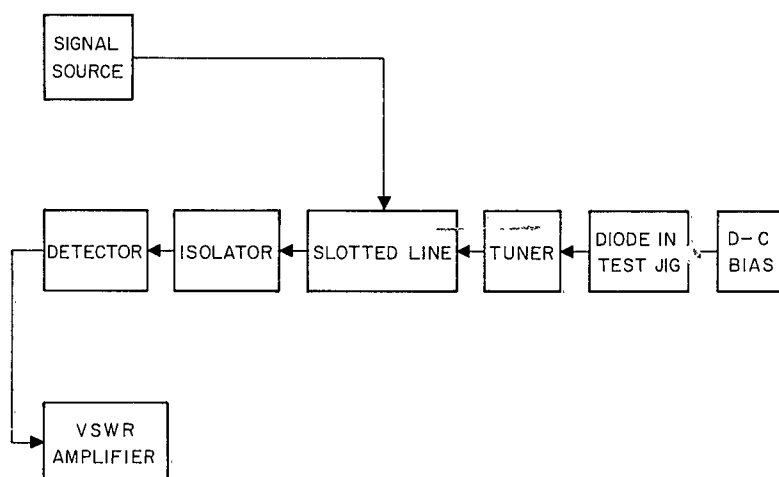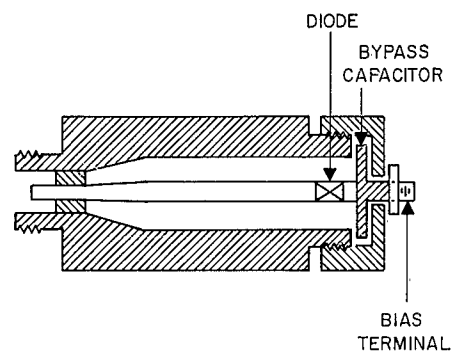
Fig. 4 Test Fixture for Measurement of Diode Characteristics
at Microwave Frequencies

Let

$$Q = \Delta x/R \qquad (1)$$

where

Δx is the change in reactance measured between
forward and reverse breakdown, and

R is the normalized transformed resistance.

The value of R remains fairly constant as a function of bias at 1300 mc.
However, as shown in Figs. 5 and 6, Δx is impossible to measure at this
frequency. Therefore, Q cannot be measured.

Fig. 6 Micro State Varactor

Fig. 5 RCA Varactor

Impedance Characteristics

Let

$$f_c = Q f_o \qquad (2)$$

where

f_o is the operating frequency.

Equation (2) shows that, in order to measure cutoff frequencies greater than 200 kmc at 1300 mc, a Q of approximately 200 is needed. This measurement is very difficult to obtain at 1300 mc and a much higher operating frequency is suggested.

Therefore, a new diode jig, designed to operate at approximately 26 kmc, was developed, necessitating Q measurements of the order of 10. This jig (Fig. 7) provides a step-transition from high to low impedance in the K_A-band waveguide. Diode characteristics measured with this jig will be reported in the next quarter.
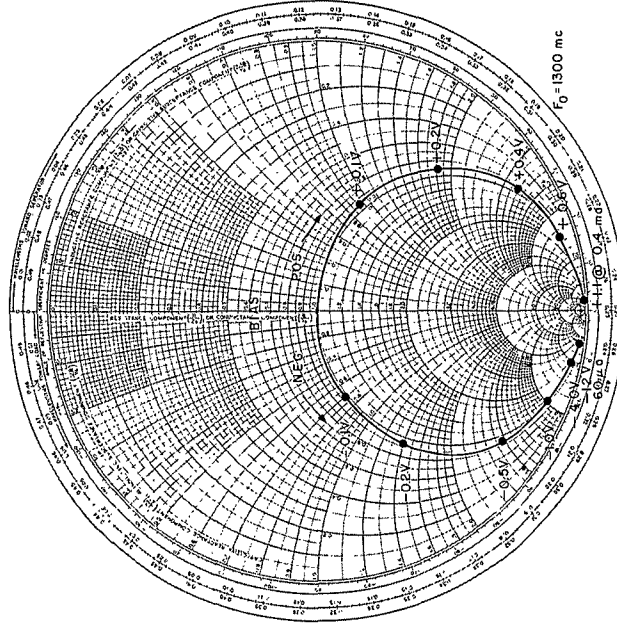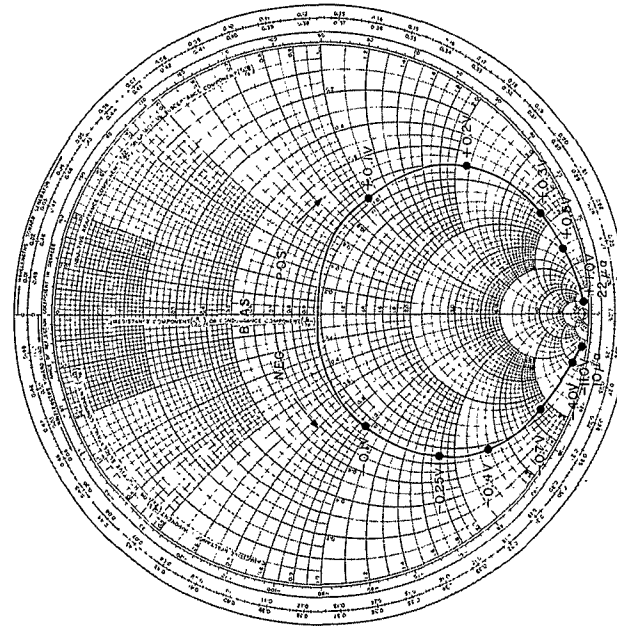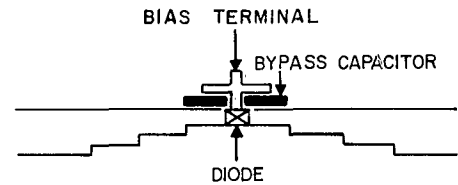
Fig. 7 Test Fixture for Measurement of Diode Characteristics at K_A-Band Frequencies

The next step was to measure the diode resistance (R_s) and capacitance (C) at a particular bias voltage at 1300 mc. An equivalent circuit was assumed for the diode and its holder (Fig. 8).[3]

Fig. 8 Equivalent Circuit for Diode Test Fixture
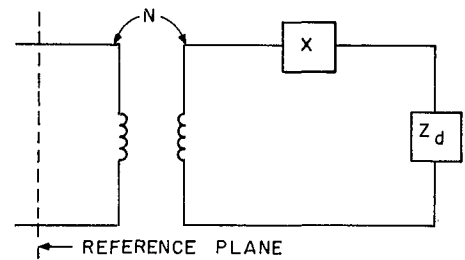
At a particular frequency the diode test fixture can be represented by a length of uniform transmission line, an ideal transformer of transformation ratio N, a series reactance X, and a diode junction impedance Z_d. This equivalent circuit is correct if the test fixture is lossless.

Three measurements are needed to evaluate the parameters of the equivalent circuit:

(a) $Z_d = \infty$ (open circuit). The location of a voltage maximum is measured to establish the reference plane (Fig. 8) at which the load is effectively located.

(b) $Z_d = 0$ (short circuit). The distance between the load reference plane and the position of a voltage minimum d_o is measured. This distance specifies the value of the product of the transformation ratio and the series reactance NX as shown in Equation (3):

$$NX = -Z_o \tan \frac{2\pi d_o}{\lambda} \tag{3}$$

where

Z_o = characteristic impedance of line, and

λ = line wavelength.

(c) $Z_d = R$ (standard resistance). The value of the transformation ratio N is obtained. From the known resistance, the input impedance at the reference plane is measured, and the resistive component of this impedance is equated to NR, (R, N are already determined).

Once the parameters of the equivalent circuit are determined, the impedance Z_d of the diode junction can be obtained. With the diode in place,

the input impedance at the reference plane is measured. The value of the load impedance, which in this case is equal to $Z_d + X$, is given by the transmission line equation:

$$Z_d + X = \frac{Z_o}{N} \frac{1 - jS \tan \frac{2\pi d}{\lambda}}{S - J \tan \frac{2\pi d}{\lambda}}$$ (4)

where

      S = voltage standing wave ratio (VSWR), and

      d = the distance from reference plane to a voltage minimum.

The resistive and reactive components of the diode junction are given by:

$$R_s = \frac{Z_o}{N} \frac{S\left(1 + \tan^2 \frac{2\pi d}{\lambda}\right)}{S^2 + \tan^2 \frac{2\pi d}{\lambda}}$$ (5)

$$X_d = -j \frac{Z_o}{N} \frac{(S^2 - 1) \tan \frac{2\pi d}{\lambda}}{S^2 + \tan^2 \frac{2\pi d}{\lambda}} - X$$ (6)

Electron-Beam Parametric Amplifier (EBPA)

      The performance characteristics of the subdepartment L-band electron beam parametric amplifier (EBPA) are still undergoing investigation, with particular emphasis on noise performance. Two methods for reducing the noise temperature of the EBPA are under consideration. Both involve the separation of the signal frequency and idler frequency, with the termination of the idler at liquid nitrogen temperature (77°K). A working paper explaining the theory of operation of the EBPA, plus experimental results, standard noise theory, experimental noise figure results, and methods by which the idler channel temperature can be reduced, is being prepared.

    W. M. Bridge   J. H. Phillips

    C. J. Ferraro   R. J. Snay

    A. P. Murphy   P. M. Ware

ANTENNA STUDIES

Shielded Horn Study

Obstacles in the radiation pattern range in the vicinity of the antenna under test were removed in order to look at regions in the pattern where the lobe structure exceeded −50 db. The effect of the chokes or wave traps was determined again under the improved conditions.

The various orientations of the horn which may be used during pattern measurements are sketched in Fig. 9. All measurements were obtained with the axis of rotation perpendicular to the earth.

With the horn oriented to place its transverse plane parallel to the earth (Fig. 9), the pattern of Fig. 10 was measured. No chokes were present on the antenna for this test. Backlobe levels are denoted. The chokes then were added and the graph of Fig. 11 measured. The backlobe levels in db down from the main lobe peak were 48.0 for the uncorrected horn and > 59.3 for the horn with chokes.

In a second set of data, the uncorrected horn pattern of Fig. 12 may be compared with the corrected horn pattern of Fig. 13. The antenna for this measurement was oriented to place the longitudinal plane perpendicular to the axis of rotation (Fig. 9). Pertinent backlobe levels in db down from the main lobe peak were 53.2 for the uncorrected horn and > 59 for the horn with chokes.

The backlobe in the transverse plane was reduced by more than 11 db and in the longitudinal plane by approximately 6 db. No effect was observed in either plane when the antenna was excited with longitudinal polarization. The location of the chokes is shown in Fig. 14. The dynamic range of the receiving system must be increased to determine the total improvement caused by the chokes.

APERTURE

E-FIELD
POLARIZER

WAVEGUIDE
INPUT

AXES OF
ROTATION

(a)
TRANSVERSE PLANE
TRANSVERSE POLARIZATION

PARABOLOIDAL
SURFACE

E-FIELD
POLARIZER

(b)
TRANSVERSE PLANE
LONGITUDINAL POLARIZATION

E-FIELD
POLARIZER

AXES OF
ROTATION

(c)
LONGITUDINAL PLANE
LONGITUDINAL POLARIZATION

(d)
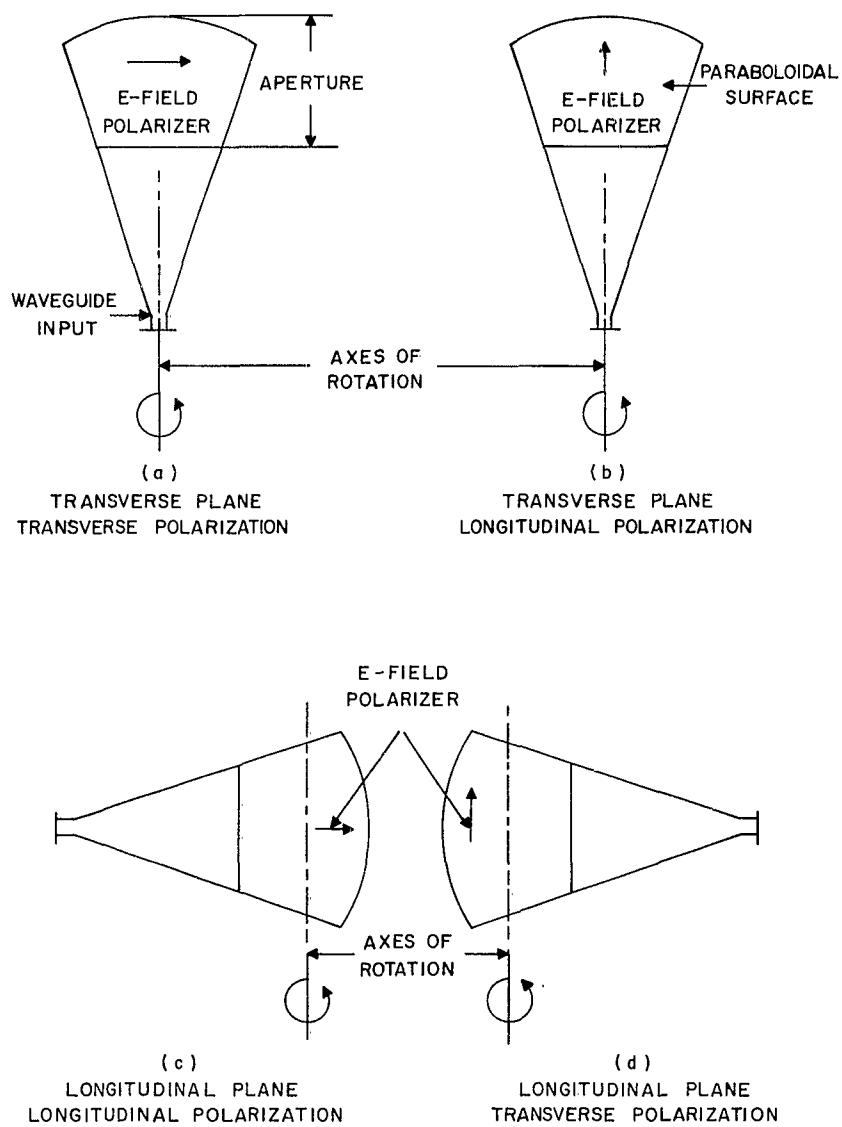LONGITUDINAL PLANE
TRANSVERSE POLARIZATION

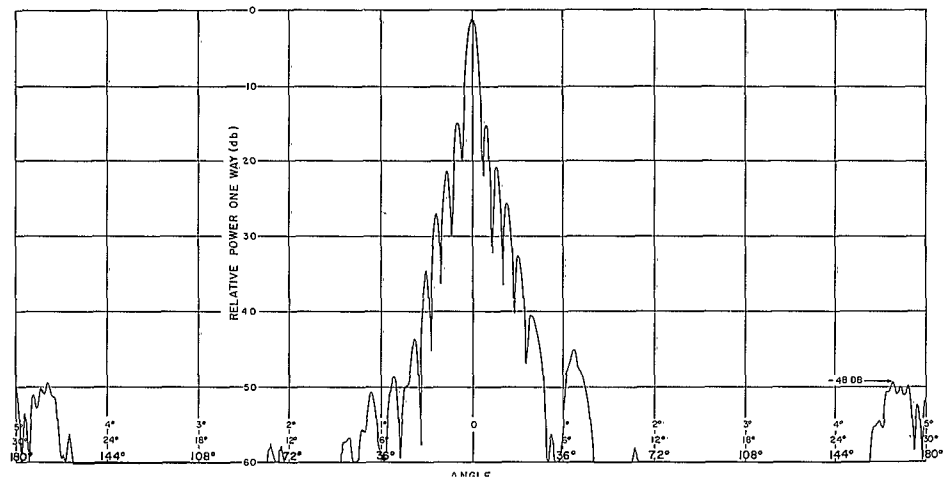Fig. 9 Orientation of Antenna During Radiation Pattern Measurements
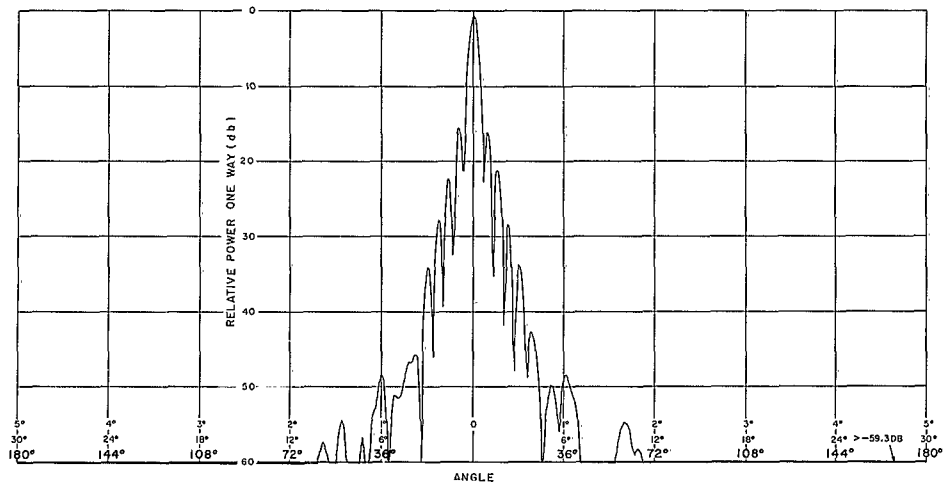
Fig. 10   No Chokes

Fig. 11   Chokes Installed

Shielded Horn Radiation Patterns
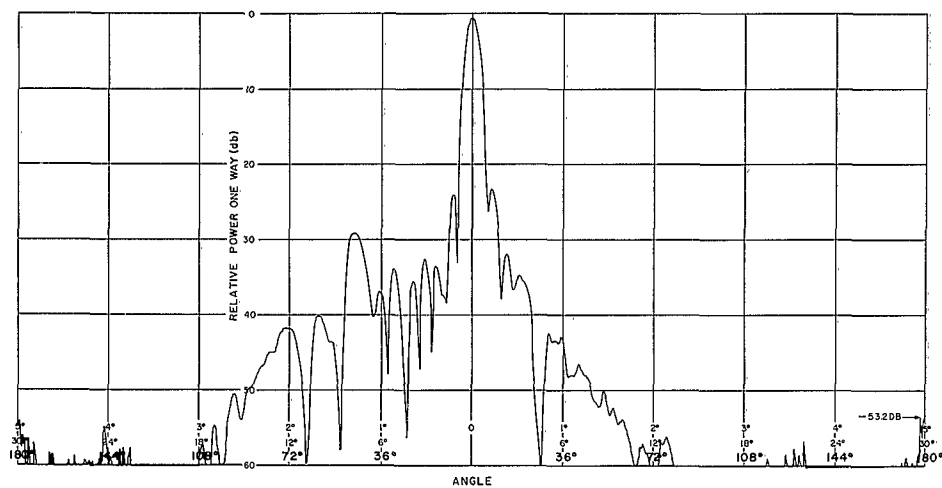Transverse Plane and Polarization;   Frequency = 9Gc

Fig. 12   No Chokes
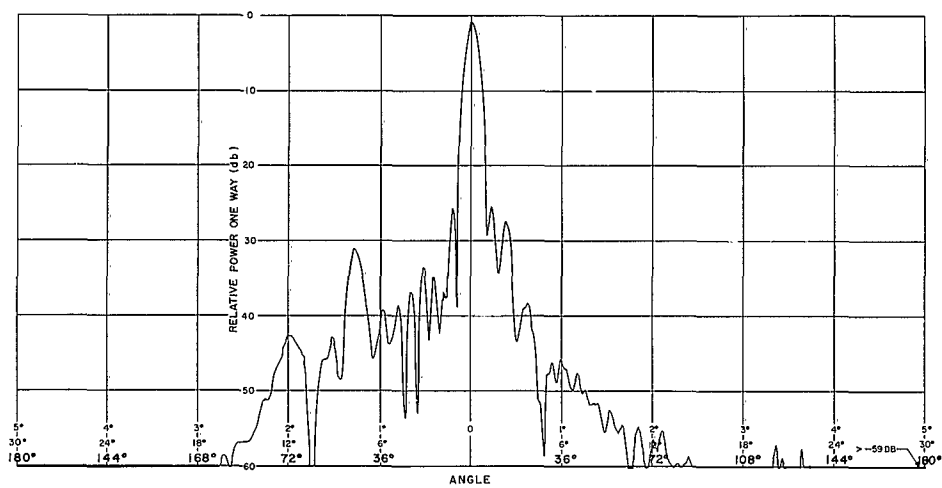

Fig. 13   Chokes Installed

Shielded Horn Radiation Patterns
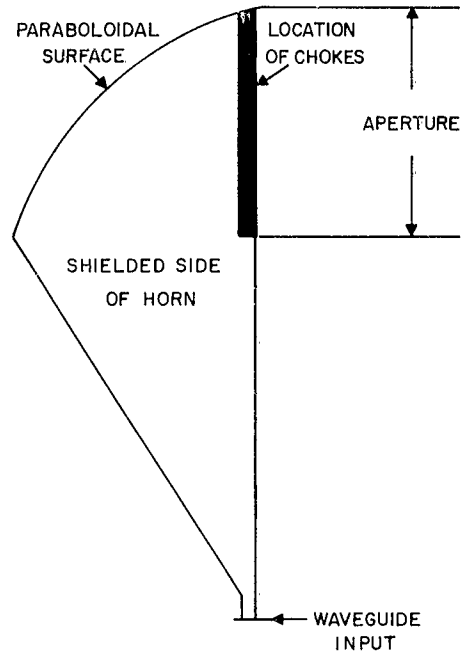Longitudinal Plane and Polarization;   Frequency = 9Gc

14

PARABOLOIDAL
SURFACE

LOCATION
OF CHOKES

APERTURE

SHIELDED SIDE
OF HORN

WAVEGUIDE
INPUT

Fig. 14 Shielded Horn (Side View)
Showing Location of Chokes

Clay Pit Hill Antenna Range

The property to be used as a transmitting site for the proposed radiation
pattern tests of the experimental radar receiving antenna was obtained under a
six-month renewable lease. A temporary tower with a parabolic transmitting
antenna was installed. A positioning device at the Boston Hill receiving site
will allow a small receiving horn to measure the amplitude variations of the
electric field in the vicinity of the aperture of the 30-foot antenna. A permanent
structure will be erected at Clay Pit Hill only after initial measurements justify
further development.

A. L. Murphy

Low-Noise Feed

Secondary pattern and gain measurements using the low-noise feed horn
modeled at X-band were completed. Pattern and gain characteristics are

summarized in Table II, and the patterns shown in Figs. 15 and 16. Table II
also lists pattern and gain characteristics, with a model feed horn optimized for
maximum gain, and Figs. 17 and 18 show these patterns.

The results obtained are not consistent with design objectives. Future
effort will be directed toward resolving this inconsistency. However, there is a
practical limit to the amount of useful information received from model meas-
urements. Pattern and impedance data alone do not provide a direct answer to
noise figure reduction. Also, it is immediately obvious that analytic calculations
of thermal noise received by an antenna are complex since these require a
complete knowledge of the location, temperature and reflection characteristics
of everything visible to the antenna, as well as knowledge of the three-dimensional
field pattern of the antenna itself.

It is the goal of this study to reduce these complexities and provide design
data by obtaining optimum signal/noise performance in parabolics.

Table II

Pattern and Gain Characteristics of Low-Noise
and Optimum Gain Feed Horns

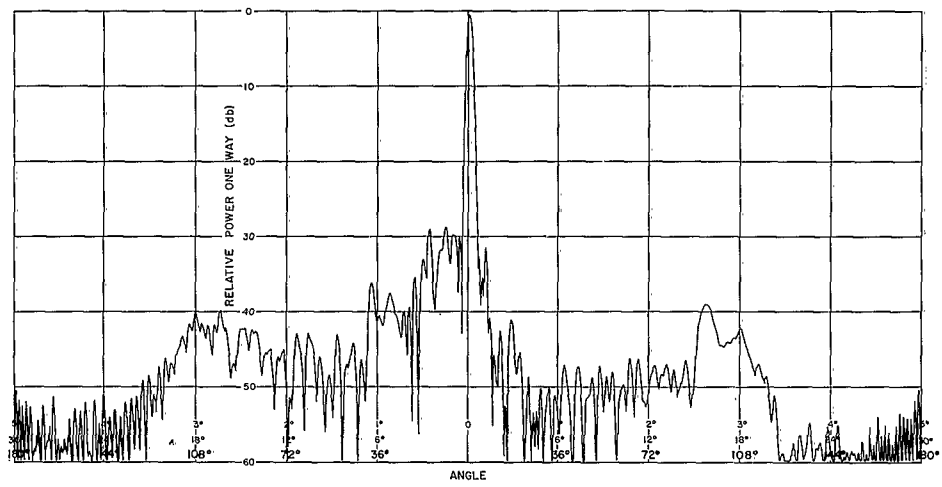| Frequency (mc)	1/2 Power BW (Deg.) E-Plane	H-Plane	First Sidelobes (db) E-Plane	H-Plane	Gain (db)
Low-Noise Feed Horn					
8890					38.0
9250	2.0	2.0	29.2	27.0	38.6
9600					39.2
Optimum Gain Feed Horn					
8890	1.7	1.8	24.1	26.1	38.1
9250	1.7	1.8	23.6	23.1	38.8
9600	1.7	1.7	22.0	26.5	39.6

16

Fig. 15 E-Plane Low-Noise Horn
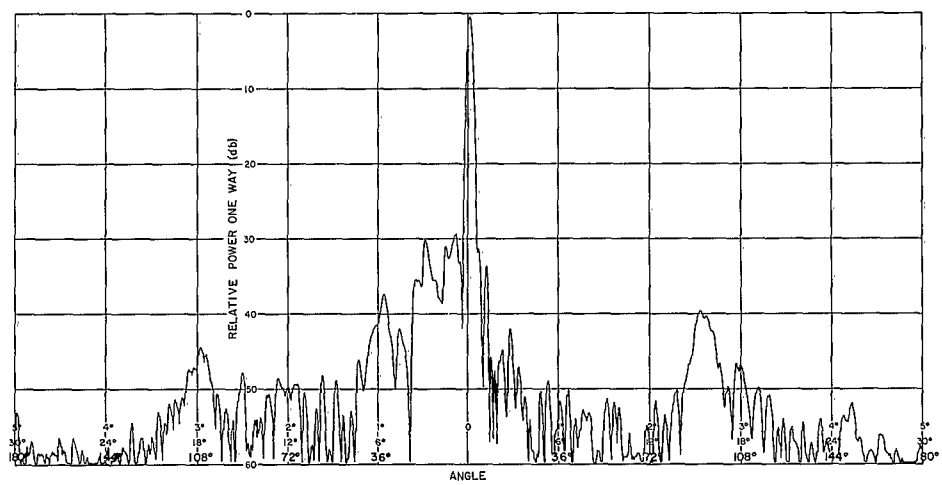

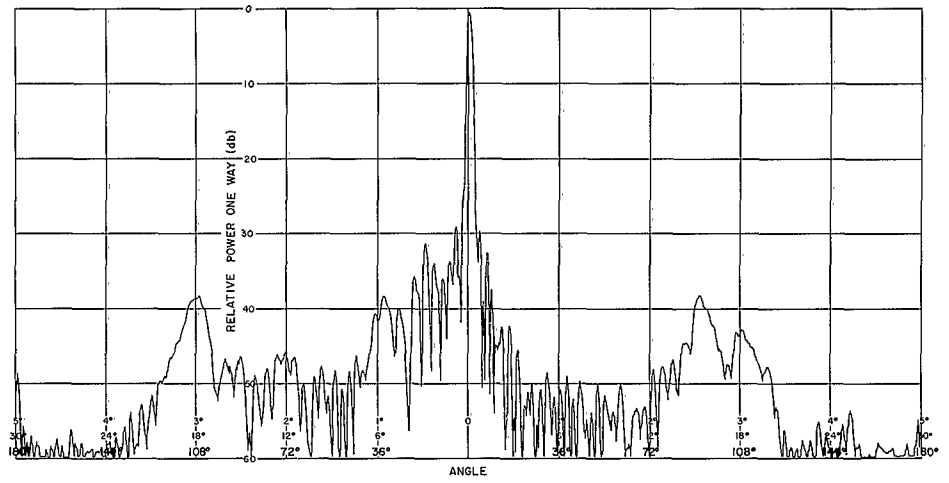Fig. 16 H-Plane Low-Noise Horn

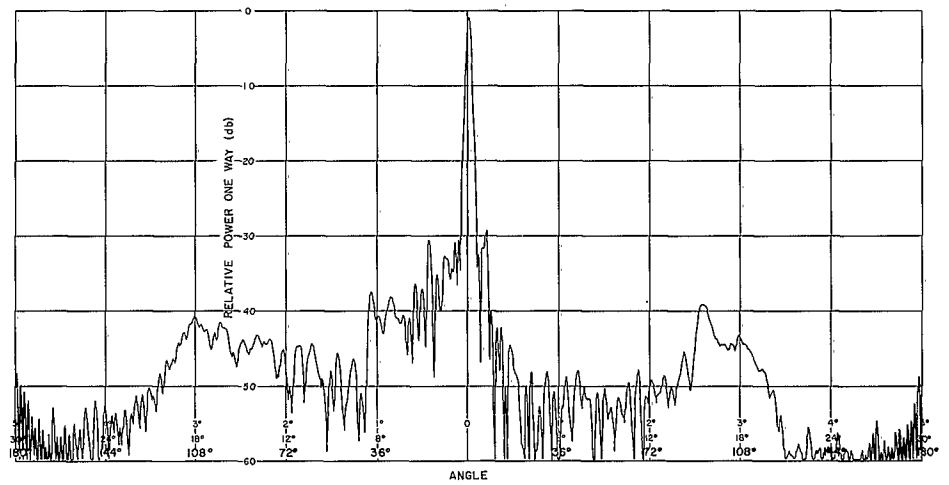Fig. 17   H-Plane Large Flanged Horn

Fig. 18   E-Plane Large Flanged Horn

18

Monopulse Development

All components were fabricated and electrically tested prior to assembly of the X-band waveguide dual-polarized monopulse comparator circuit. The quartile transducer is shown in Fig. 19.
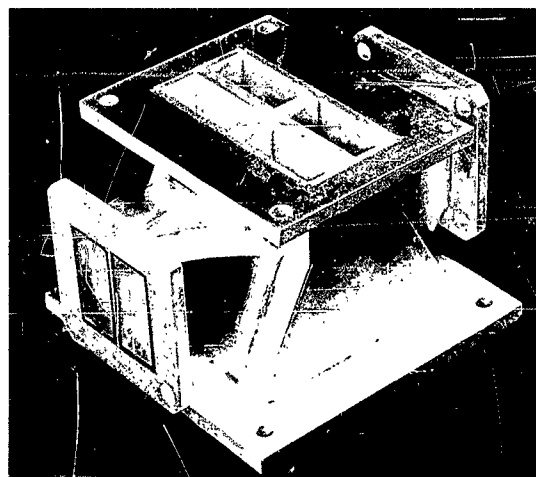

Fig. 19 Quartile Transducer

During the last quarter, it was determined that the receive-only tracker at Boston Hill would be modified and updated using a cassegrainian four-horn monopulse feed system. An L-band packaged comparator circuit of standard WR650 waveguide was ordered from I-T-E, Circuit Breaker, Philadelphia. Delivery is promised for late December.

The cassegrainian subreflector was modeled and positioned with a horn-lens combination feed. The subreflector and feed are shown under test in Fig. 20. The subreflector chosen has a 3 percent aperture block of the main dish. This provides a reflector sufficiently large for optimum illumination of the difference channel mode in monopulse operation.

Future plans include development of a four-horn cluster for efficient illumination of the subreflector.
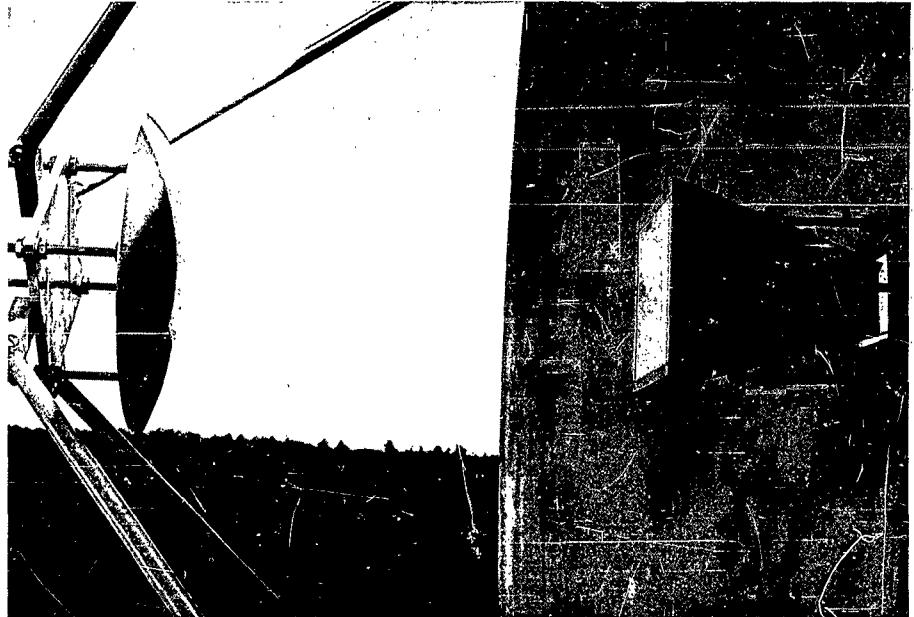
Fig. 20 Subreflector and Feed for Cassegrainian System

Model Antenna Pattern Range

Increased efficiency was accomplished during the last quarter when the transmit location of the 350 model antenna pattern range was converted entirely to remote control operation. Now all pattern measurements can be taken from the receive location by one operator who adjusts the transmitter as required. All control functions were removed; polarization, elevation, and azimuth positioning and oscillator adjustments are now controlled from the receive location. The transmit oscillator is controlled by a klystron power supply located at the receive location, with the control cables driving a waveguide klystron located behind the transmit dish. Frequency changes are accomplished by a synchro-controlled motor as are polarization and el-az adjustments.

The receive and transmit locations are shown in Figs. 21 and 22.
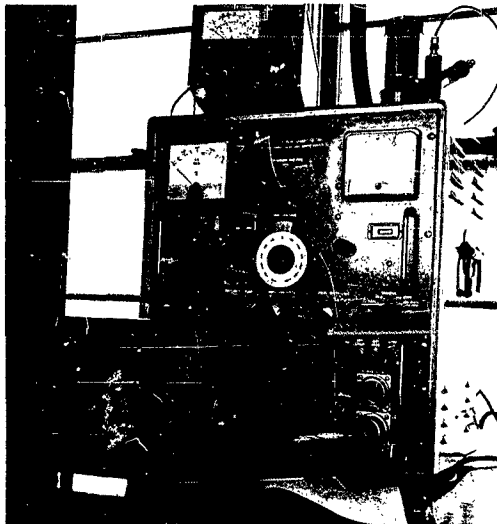
D. E. Cozzens

Fig. 21 Receive Location for
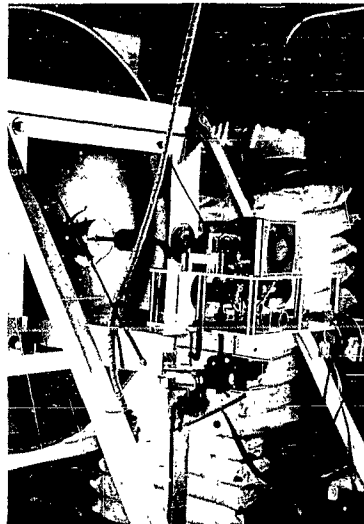350 Model Antenna
Pattern Range

Fig. 22 Transmit Location for
350 Model Antenna
Pattern Range

LASER STUDIES AND TECHNIQUES

Design and Construction

The design and testing of the 2000-joule power supply was completed. The trigger-charger unit (Fig. 23), when used with an external dc digital voltmeter, can charge the capacitor bank to 4000 volts with $\pm$ 2 percent accuracy. The capacitor bank, also shown in Fig. 23, contains four 240-microfarad capacitors in parallel, with provisions for disconnecting any one or more from the line. Each capacitor measures to an accuracy of $\pm$ 2 percent. Either a 0.3 or a 0.6-millihenry choke can be easily inserted in the discharge path. The d-c resistance of these chokes and the current-carrying leads were measured. Four 25-microfarad capacitors, calibrated to within $\pm$ 2 percent, are also available. The power supply (Fig. 24) is capable of flashing the E. G. & C. type FX-100, FX-38, FX-42, FX-45, and FX-47 flash tubes.

Fig. 23 Laser Trigger-Charger
Unit and 2000-Joule
Capacitor Bank

Two types of elliptical cavities were designed and constructed. One, which is almost circular, has major and minor diameters of 5.000 and 4.976 inches, respectively. This unit (Fig. 25) is equipped with adjustable mounts so that the laser rod and the flashtube can be positioned accuractely along the focal lines. The other cavity (Fig. 26) has major and minor diameters of 5.000 and 4.000 inches, respectively. At present, it is equipped with fixed mounts Adjustable mounts, currently being fabricated, have undergone preliminary testing.

A vacuum-jacketed double wall Pyrex glass dewar in which the laser rod can be mounted was obtained. Cryogenic cooling is provided by first passing dry nitrogen gas through a copper coil immersed in an open dewar of liquid nitrogen and then into the glass dewar and along the laser rod. The technique is outlined in Fig. 27. Preliminary tests only have been performed.
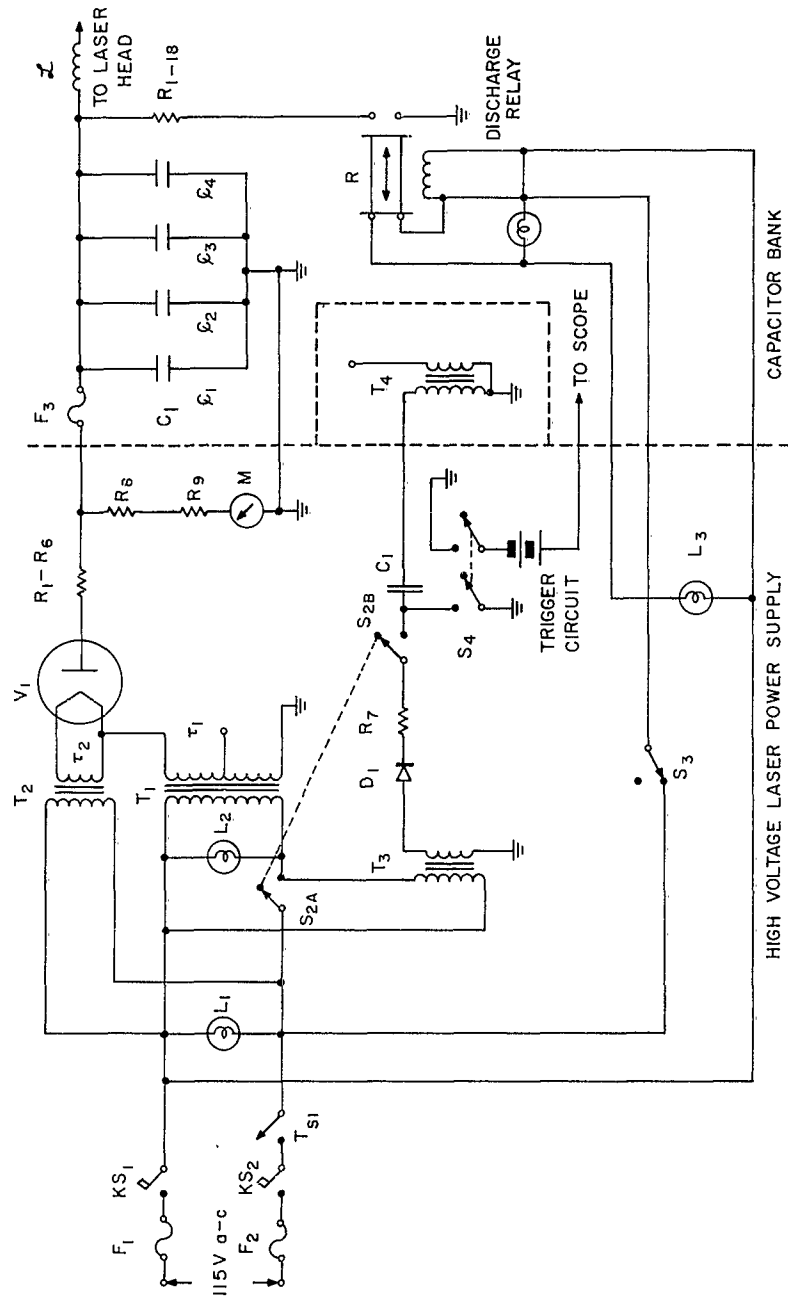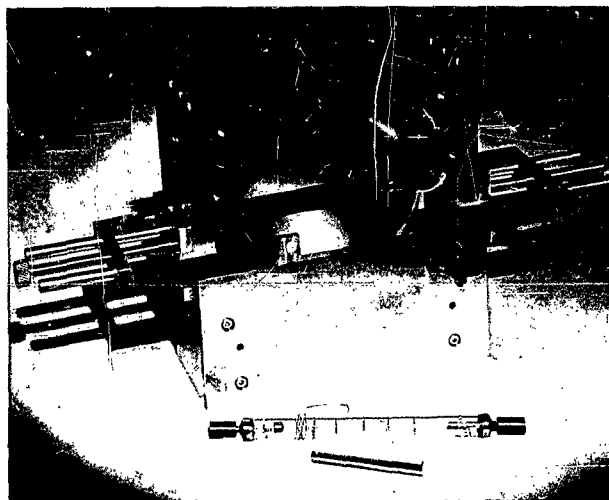
Fig. 24 Diagram of 2000-Joule Power Supply

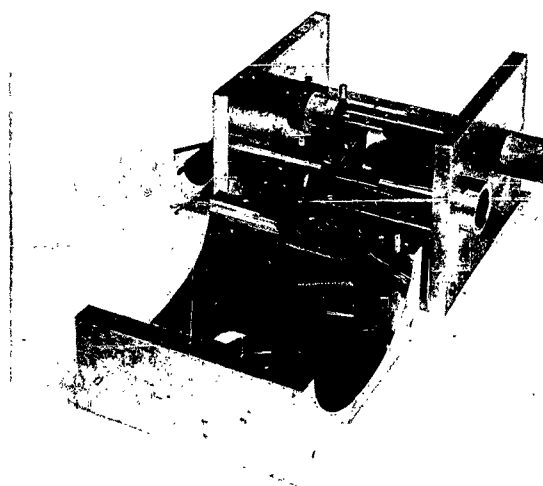Fig. 25 Adjustable Mounts, Flash Tube and Ruby Rod

Fig. 26 Fixed Mounts, Flash Tube and Ruby Rod Installed

ELLIPTICAL LASER CAVITY

GLASS VACUUM DEWAR

N₂ (77°K)

N₂ (300°K)

RUBY ROD
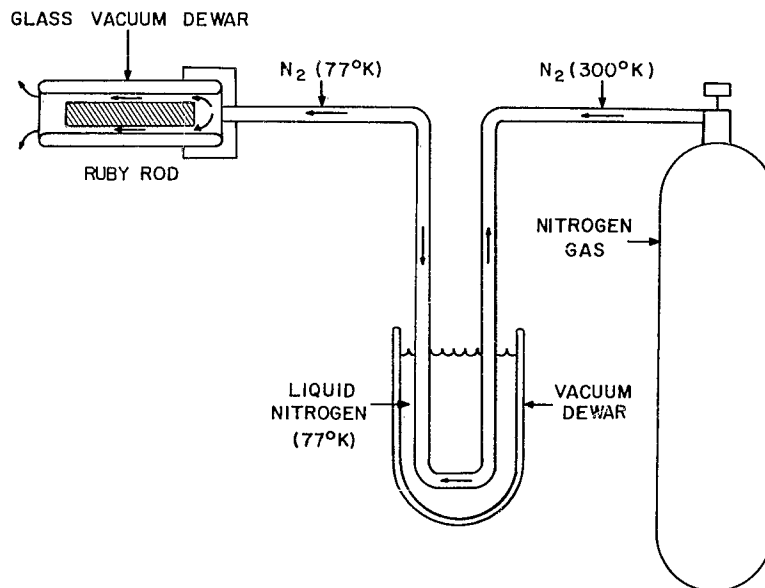
NITROGEN
GAS

LIQUID
NITROGEN
(77°K)

VACUUM
DEWAR

Fig. 27 Apparatus for Cryogenic Cooling of Ruby Rod

A phototube detector mount and amplifier (Fig. 28) was built and tested. A 1P39 phototube (S-4 response, 4000 A peak) and a 925 phototube (S-1 response, 8000 A peak) are provided for optically detecting the intensity of the xenon flash tube and the ruby output, respectively.

A calorimeter (Fig. 29) capable of measuring pulsed laser output energy in the range 0.1 to 1 joule is being constructed. The small carbon cone and its thermally insulated mount are shown in Fig. 30. The heating due to a single laser pulse is measured by a thermistor bridge and pen recorder. Calibration is provided by recording the heating due to the discharge of a known amount of energy through the cone from a capacitor. Ambient temperature compensation is provided by an additional thermistor in the bridge, resulting in an estimated accuracy of ± 10 percent.

Design of a variable delay trigger circuit for oscilloscope synchronization with the flash tube is in the breadboard stage.
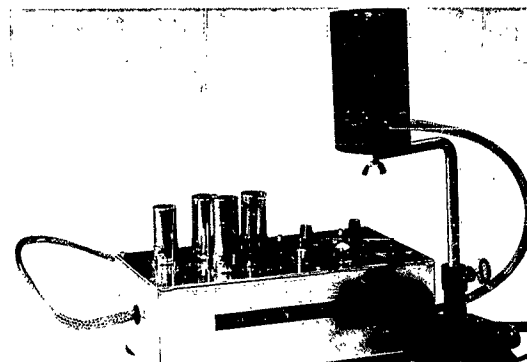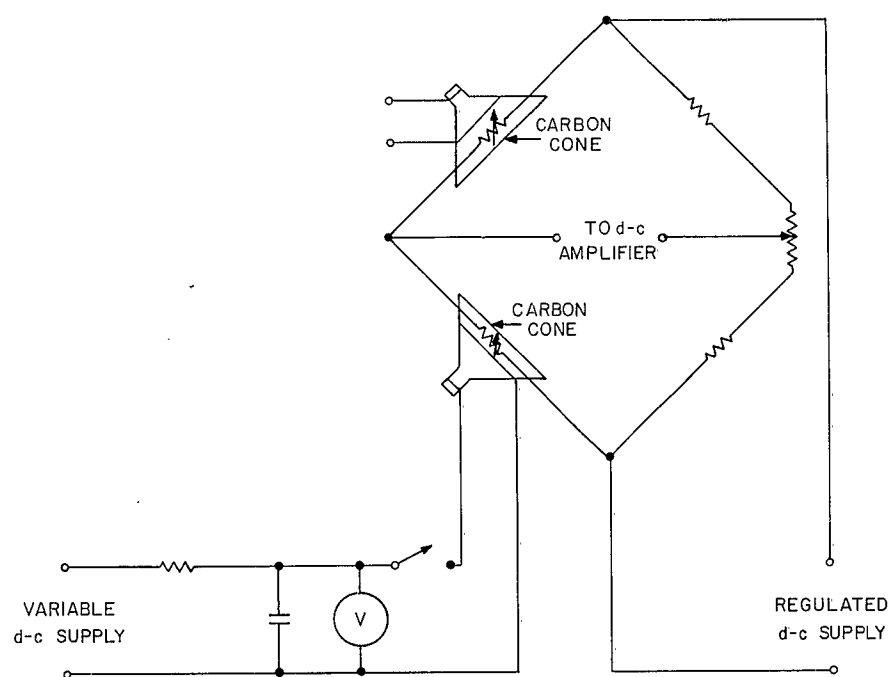
Fig. 28 Phototube Detector Mount
and Amplifier

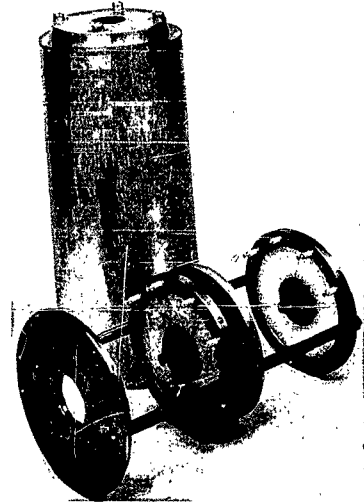Fig. 29 Basic Schematic of the Calorimeter

Fig. 30 Thermally Insulated Calorimeter
Mount and Carbon Cones

Experimental Results

A graph of the optical pump output intensity versus time is shown in
Fig. 31. The 1P39 phototube is a distance of 6 feet from the laser for a dis-
charge of 200 joules from a 117-microfarad capacitor through a 0.3 millihenry
choke and two type FX-100 flash tubes in series. The interval between the
one-third intensity points is 250 to 300 microseconds. The leading edge plateau
and the multitude of spikes are caused by magnetic induction from the discharge
current. The magnitude of this induction prevents the satisfactory measurement
of the flash tube voltage drop and current shapes.

Fig. 32 is a plot of the measured threshold (in terms of the number of
joules stored in the capacitor bank) at room temperature for a 2-inch long by
0.250-inch diameter ruby, and a 2-inch long by 0.160-inch diameter ruby. The
latter has a 0.070-inch thick sapphire overlay. The optic axes of both are
oriented at 90 degrees with respect to the rod axis, and both have dielectric
coated ends. The former contains 2.45 times more ruby due to its larger cross
section. To obtain the curves, two FX-100 flash tubes were placed parallel to
and touching the ruby from opposite sides. The combination was wrapped with
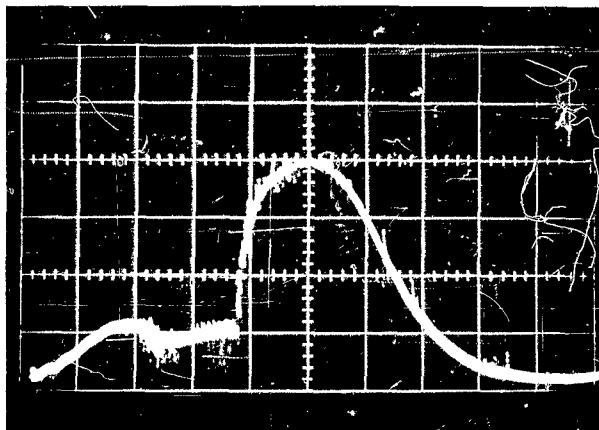aluminum foil.

Fig. 31   Optical Pump Output Intensity (Arbitrary Units)
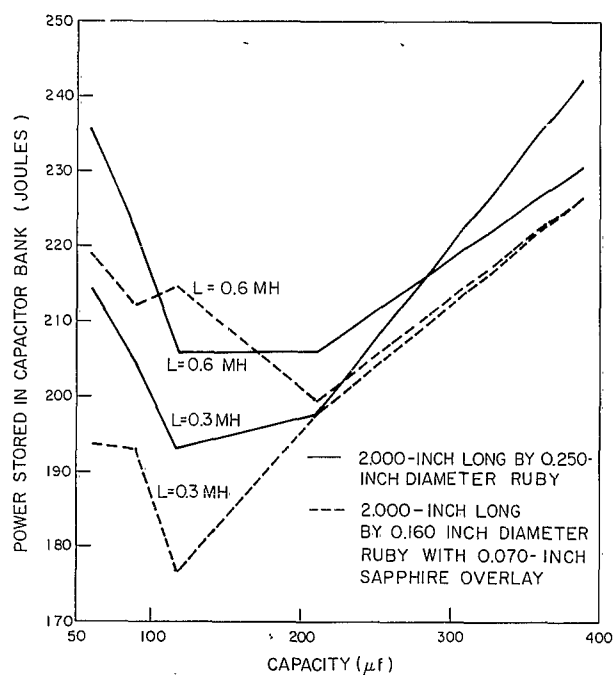vs Time (100 μsec/cm) of Two Flash Tubes in Series

Fig. 32   Energy Required for Lasing Threshold for Various
L-C Combinations in Flash Tube Unit

The threshold dependence on capacity and inductance is apparent from Fig. 32. The variation arises from the variation in flash tube peak intensity and duration of capacity and inductance. Also, the threshold of the sapphire overlay is not lower than that of the larger ruby in proportion to the volume ratios. This may be due in part to inadequate pump coupling since the flash tubes are separated from the ruby by the thickness of the sapphire overlay. However, this is offset somewhat by the focusing action of the sapphire. Inasmuch as the sapphire overlay was observed to lase out both of its ends simultaneously with comparable intensities and with appreciable beam divergence, it may be that both dielectric coatings inadvertently were made partially transmissive. This, plus the fact that the ends cannot be visually distinquished from each other as is possible with the larger ruby, would account for a higher threshold . The coatings will have to be replaced in order to confirm this.

Program for Next Quarter

During the next quarter the elliptical cavities and the calorimeter will be tested. Also planned is the retesting of the sapphire overlay with new dielectric coatings and threshold measurements at liquid nitrogen temperatures. Additional quantitative tests to be performed include coherence, output spectrum measurement and output waveform.

<div style="text-align: right">

R. D. Gallagher

A. P. Murphy

P. M. Ware

</div>

PERIODIC STRUCTURES

During this quarter, a study of various types of periodic structures was started to determine which type will yield the highest amount of slowing with a minimum of loss. Slowing factor is defined as the ratio of the velocity of light to the group velocity.

Three well-known methods of producing slow waves exist:

(a) Dielectric slowing — Meander line (simplest type)

(b) Resonant slowing — Karp structure, Interdigital line

(c) Geometric slowing — Helix

In general, dielectric slowing has the highest loss of the three types due to the presence of the dielectric material. In this case the slowing factor S is approximately equal to $\sqrt{\epsilon_r}$, where ϵ_r is the relative dielectric constant. For example, Titanium Dioxide has a dielectric constant of 100, which gives a slowing factor of 10.

The simplest example of geometric slowing is the helix. In this case the wave travels along the helix wire at the velocity of light, and the axial phase velocity is reduced in proportion to the number of turns per wavelength.

Various types of ladder structures, such as the interdigital line and the Karp, are examples of resonant slowing. Each period of the ladder structure is a resonant element and the energy is reflected back and forth between the side walls. The period of the propagating structure must be small for broadband and high slowing operation. The group velocity v_g is given by:

$$v_g = \frac{d\omega}{d\beta} \approx \frac{\Delta\omega L}{\Delta\beta L} = \frac{2\pi L \Delta f}{\Delta\beta L} \tag{7}$$

where

L   is the period, and

Δf is the bandwidth.

The operating passband for the fundamental mode of a periodic structure is $0 \leq \beta L \leq \pi$. Therefore, $\Delta\beta L = \pi$. Substitution in (7) gives:

$$v_g = 2L\Delta f = \frac{c}{S} \tag{8}$$

30

Then

$$S = \frac{c}{2L\Delta f} = \left(\frac{\lambda_o}{2L}\right)\frac{f_o}{\lambda_f} \tag{9}$$

Equation (9) shows that for a large bandwidth and high slowing, period L must be small.

Another type of slowing, not as well-known, is dispersive slowing. Here the group velocity is made small by operating on the cutoff characteristic of a microwave filter. At the cutoff frequency of any filter, $d\omega/d\beta$ is very small. The Q of the filter must be high if the insertion loss is to remain low.
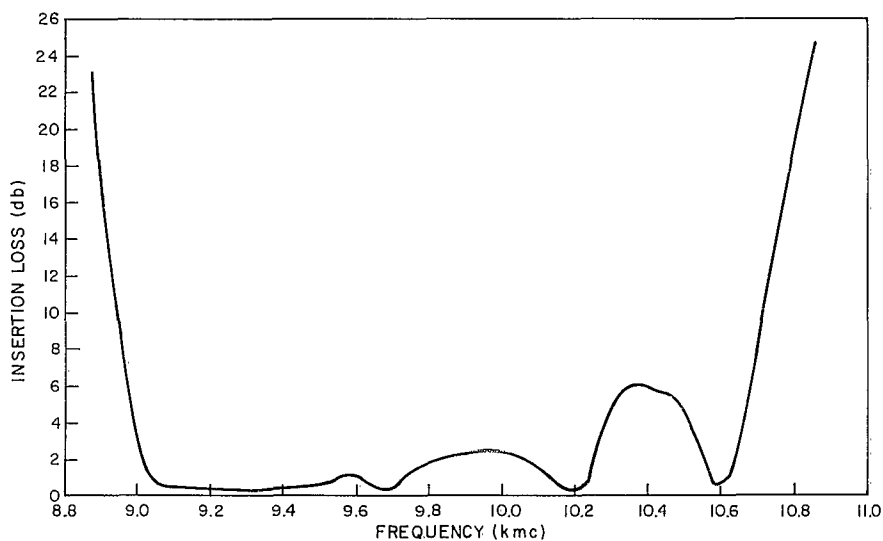

Fig. 33 Insertion Loss vs Frequency

The first type of resonant slowing structure analyzed was an X-band waveguide loaded with seven 0.062-inch diameter inductive posts with 0.700-inch

spacing. Fig. 33 is a plot of the passband characteristic of the periodic structure operating in its fundamental mode. The total phase shift through the device as a function of frequency is shown in Fig. 34. The theoretical and measured $\omega - \beta$ diagrams are shown in Fig. 35. Point (A) in Fig. 35 corresponds to a frequency of 9.7 kmc and, at this point, the phase velocity (v_p) is 3.76×10^{10} cm/sec while the group velocity v_g is approximately given by $\Delta \omega / \Delta \beta = 0.427 \times 10^{10}$ cm/sec. The slowing factor is then $S = c/v_g \approx 7.0$.

The second type of periodic structure to be studied is the capacitively loaded waveguide; this will be reported in the next quarter.
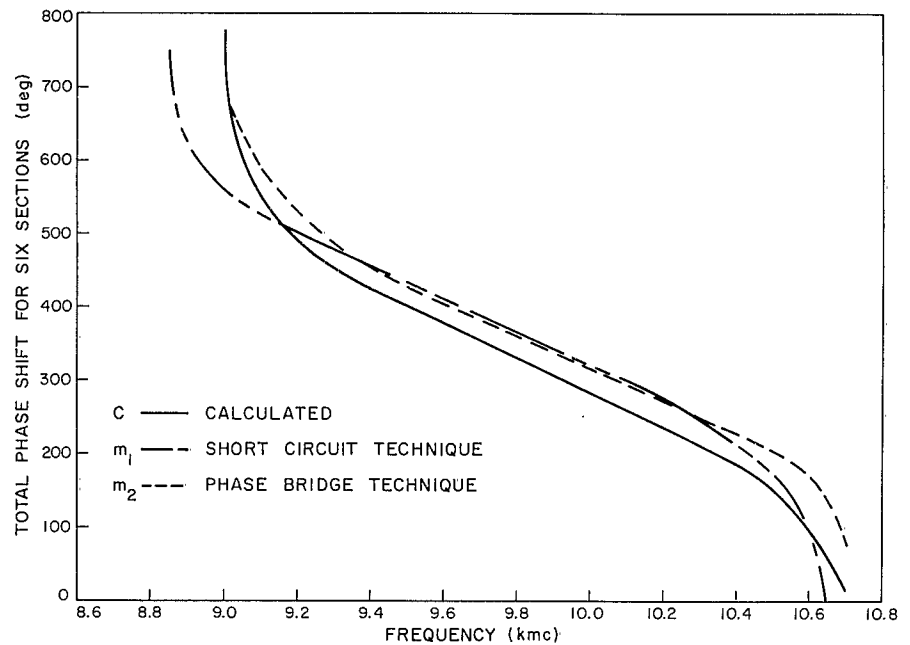
<div align="right">R. J. Snay</div>

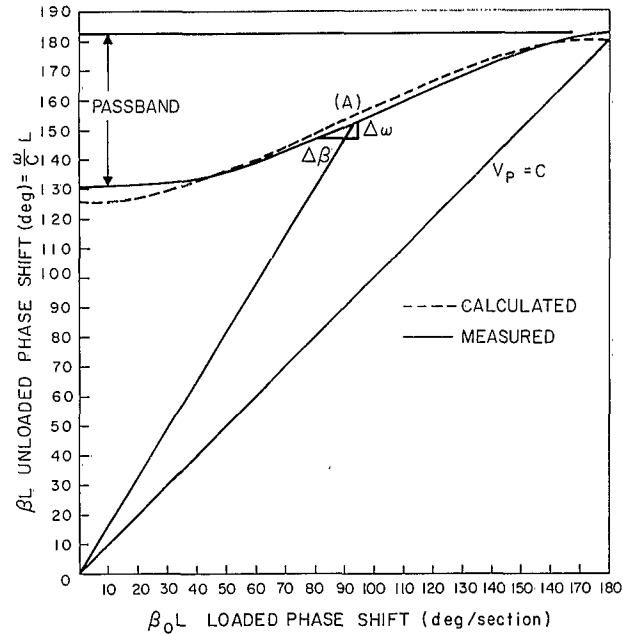Fig. 34 Total Phase Shift vs Frequency

Fig. 35 βL Unloaded Phase Shift vs $\beta_o L$ Loaded Phase Shift

MICROWAVE TUNNEL DIODE AMPLIFIER

The effect on the microwave tunnel diode amplifier program was curtailed during this past quarter due to two problems. The first problem was the difficulty in obtaining tunnel diodes with the necessary parameters for use in the present amplifier design. The second problem was that of obtaining a ferrite circulator with the proper VSWR, insertion loss, and isolation characteristics necessary for the successful operation of the tunnel diode amplifier. Both problems appear to be solvable with state-of-the-art techniques now available. Effort will be directed during this quarter towards perfecting a broad band amplifier that will be more stable and that will have better noise performance than previous models. Also planned is a design for making a voltage tuned version utilizing a varactor as the tuning element for frequency jumping techniques.

R. D. Gallagher

MICROWAVE FERRITE LIMITERS

A report on ferrite microwave limiters is currently being published. This report is an instructional survey of the present-state-of-the-art including theory, published results, and experimental work performed in this laboratory.

R. L. Severance

PHASE MEASUREMENTS

The redesign of some of the components in the phase measuring system was necessary to make it compatible with the new 5.0-mc display unit. The design, building, and testing of these components is completed. As soon as technician help is available, the remainder of the phase measuring system will be completed.

C. J. Ferraro

REFERENCES

1.   Phillips, J.H., R.D. Gallagher and W.M. Bridge, "The Critically Coupled Filter at Microwave Frequencies," MTS No. 4, May 1961.

2.   Houlding, N. "Measurement of Varactor Quality," _Microwave J._, Vol. 3, No. 1, Jan. 1960, pp. 40-45.

3.   Kotzebue, K.L., "A Semiconductor-diode Parametric Amplifier." California: Stanford University Electronics Laboratories, 1960.

4.   Rowe, J.E. "Solid-State Microwave Amplifiers and Oscillators." Ann Arbor: University of Michigan, Department of Electrical Engineering Summer Course, 1961.

Hq. ESD, L.G. Hanscom Field, Bedford, Mass.
Rpt. No. ESD-TDR-63-181. RADAR SYSTEMS AND TECHNIQUES DEPARTMENT, MICROWAVE TECHNIQUES SUBDEPARTMENT QPR, JULY 1, 1962 - SEPTEMBER 30, 1962. Progress report, May 1963, 40p. incl. illus., 4 refs.

Unclassified Report

This document reports the progress of the Microwave Techniques Subdepartment from July 1, 1962 to September

1. Microwave networks
2. Microwave relay systems
3. Microwave equipment
I. Projects No. 750, 602
II. Contract AF33(600)-39852
III. The MITRE Corporation Bedford, Mass.

Hq. ESD, L.G. Hanscom Field, Bedford, Mass.
Rpt. No. ESD-TDR-63-181. RADAR SYSTEMS AND TECHNIQUES DEPARTMENT, MICROWAVE TECHNIQUES SUBDEPARTMENT QPR, JULY 1, 1962 - SEPTEMBER 30, 1962. Progress report, May 1963, 40p. incl. illus., 4 refs.

Unclassified Report

This document reports the progress of the Microwave Techniques Subdepartment from July 1, 1962 to September

1. Microwave networks
2. Microwave relay systems
3. Microwave equipment
I. Projects No. 750, 602
II. Contract AF33(600)-39852
III. The MITRE Corporation Bedford, Mass.

Hq. ESD, L.G. Hanscom Field, Bedford, Mass.
Rpt. No. ESD-TDR-63-181. RADAR SYSTEMS AND TECHNIQUES DEPARTMENT, MICROWAVE TECHNIQUES SUBDEPARTMENT QPR, JULY 1, 1962 - SEPTEMBER 30, 1962. Progress report, May 1963, 40p. incl. illus., 4 refs.

Unclassified Report

This document reports the progress of the Microwave Techniques Subdepartment from July 1, 1962 to September

1. Microwave networks
2. Microwave relay systems
3. Microwave equipment
I. Projects No. 750, 602
II. Contract AF33(600)-39852
III. The MITRE Corporation Bedford, Mass.

Hq. ESD, L.G. Hanscom Field, Bedford, Mass.
Rpt. No. ESD-TDR-63-181. RADAR SYSTEMS AND TECHNIQUES DEPARTMENT, MICROWAVE TECHNIQUES SUBDEPARTMENT QPR, JULY 1, 1962 - SEPTEMBER 30, 1962. Progress report, May 1963, 40p. incl. illus., 4 refs.

Unclassified Report

This document reports the progress of the Microwave Techniques Subdepartment from July 1, 1962 to September

1. Microwave networks
2. Microwave relay systems
3. Microwave equipment
I. Projects No. 750, 602
II. Contract AF33(600)-39852
III. The MITRE Corporation Bedford, Mass.

30, 1962. The work of the Subdepartment centers on the design, fabrication, and evaluation of microwave techniques and components which have application to long-range radar and communication problems.

IV. Microwave Techniques Subdepartment
V. PM-22 #17
VI. In DDC collection

30, 1962. The work of the Subdepartment centers on the design, fabrication, and evaluation of microwave techniques and components which have application to long-range radar and communication problems.

IV. Microwave Techniques Subdepartment
V. PM-22 #17
VI. In DDC collection

30, 1962. The work of the Subdepartment centers on the design, fabrication, and evaluation of microwave techniques and components which have application to long-range radar and communication problems.

IV. Microwave Techniques Subdepartment
V. PM-22 #17
VI. In DDC collection

30, 1962. The work of the Subdepartment centers on the design, fabrication, and evaluation of microwave techniques and components which have application to long-range radar and communication problems.

IV. Microwave Techniques Subdepartment
V. PM-22 #17
VI. In DDC collection